

High-Energy Electron Scattering from Lithium-6*

GEORGE R. BURLERSON AND R. HOFSTADTER

Department of Physics and High-Energy Physics Laboratory, Stanford University, Stanford, California

(Received July 7, 1958)

The Li^6 nucleus has been studied at 426 Mev by electron scattering methods between laboratory angles of 33° and 57.5° . Absolute values of the Li^6 cross sections have been obtained by comparison with scattering measurements made on the proton at 426 Mev and 40° . Unique values of the experimental form factors are given in tabular form. The results are analyzed in terms of various possible charge distributions. Several examples of models showing a good fit are presented and appropriate radius and skin thickness values are given. Several unsuccessful models are also discussed.

I. INTRODUCTION

EXPERIMENTS on the elastic scattering of electrons from Li^6 nuclei have been described briefly.^{1,2} Descriptions of these results have also been given in two review articles by one of the present authors.^{3,4} In references 2 and 4 the results of an analysis of the shape of the angular distribution curve were given in terms of a harmonic-well model of the Li^6 nucleus. More recent findings at 426 Mev, reported in the present paper, include absolute cross-section data and permit a much better definition of the charge distribution in Li^6 . These data show that the rms size reported in references 2 and 4 must now be increased. The new data also demonstrate that the harmonic-well model (without a cutoff of the well) cannot be made to fit the data. Acceptable models of the charge distribution in the ground state of the Li^6 nucleus will be given in this paper. The charge distributions given here are obtained from a determination of *absolute* as well as relative cross sections. The results given below provide uniquely determined form factors for Li^6 .

II. METHOD

The experimental apparatus has already been described on several occasions.^{3,5} The Li^6 target material was obtained on loan from the Oak Ridge National Laboratory and consists of 95.7% Li^6 and 4.3% Li^7 . The target thicknesses used were 497 mils, 472 mils, and 183 mils. The targets were usually scraped clean before each run to avoid oxygen contamination on the surface.

Figures 1 and 2 show the types of elastic peaks observed in these investigations. The positions of the Li^6

peaks vary as a function of angle because of the effects of recoil. A small impurity peak, perhaps due to oxygen, appears near position 20.25 in Fig. 1. The scattering from the first excited level is also shown in that figure. The shifting of energy of the Li^6 peak with angle in the predicted way serves as an aid in identifying it. Inelastic level scattering corresponding to oxygen or other impurities has not been observed in a consistent manner and is not thought to be present in appreciable amount.

Two methods were used to compute the relative cross sections. The first was based on a measurement of the areas under the peaks. The method used to define the areas is indicated by the dashed lines in Figs. 1 and 2; these were drawn so as to give the peak a roughly symmetrical shape. A radiative correction³ was applied to these data. As a check, another calculation of the relative cross sections was made and was based simply on the relative peak heights. The experimental points in the angular distribution as calculated by the area method were found to be somewhat more scattered than those calculated by the peak height method, but within the experimental errors no difference between the angular distribution curves defined by the two sets

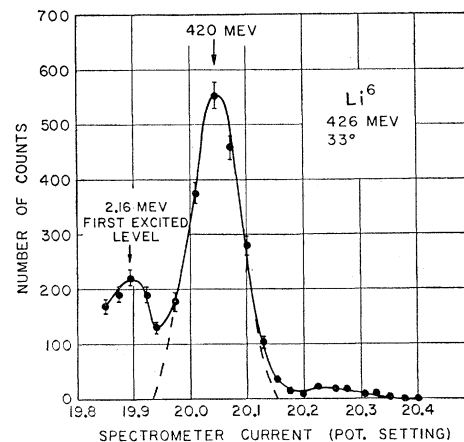


FIG. 1. The Li^6 elastic peak observed at 426 Mev and 33° . The abscissa is the voltage across a shunt in the spectrometer circuit as measured on a potentiometer, and is related to the energy of the scattered electrons. The counts observed above a potentiometer setting of 20.15 are probably due to impurities of Li^7 and oxygen.

* The research reported here was supported jointly by the Office of Naval Research and the U. S. Atomic Energy Commission and by the U. S. Air Force, through the Office of Scientific Research of the Air Research and Development Command.

¹ J. F. Streib, *Phys. Rev.* **100**, 1797(A) (1955). Streib's more recent interpretation of his data favored a large rms radius of Li^6 ; it is very satisfying that our present results are in good agreement with his recent determinations.

² R. Hofstadter and G. R. BurlerSON, *Bull. Am. Phys. Soc. Ser. II*, **2**, 390 (1957).

³ R. Hofstadter, *Revs. Modern Phys.* **28**, 214 (1956).

⁴ R. Hofstadter, *Annual Review of Nuclear Science* (Annual Reviews, Inc., Stanford, 1937), Vol. 7, p. 231.

⁵ E. E. Chambers and R. Hofstadter, *Phys. Rev.* **105**, 1454 (1956); also F. Bumiller and R. Hofstadter (to be published).

of points could be seen. To compare with theoretical cross section curves the two sets of points were averaged together.

For "absolute" calibration of the Li^6 data the electron scattering peak from the proton was observed under the same experimental running conditions as the Li^6 data. The absolute value of the proton elastic cross section is known from other electron scattering determinations.⁵ Figure 3 shows the "proton" peak observed at 40° in CH_2 and the carbon background from an equivalent carbon target. It will be noticed that the proton peak is considerably wider than the Li^6 peak. The additional width is due to the larger recoil shift of the lighter mass and corresponds to the angular width

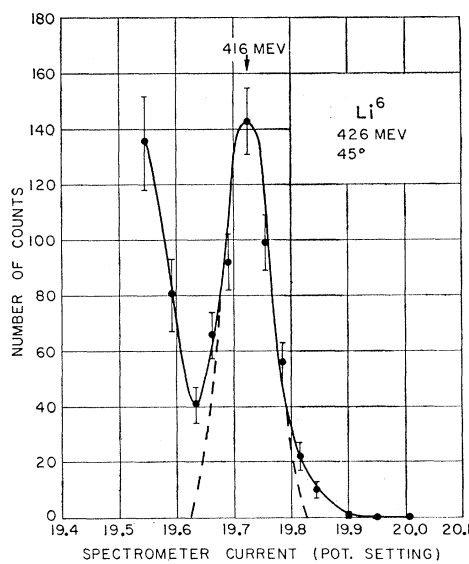


FIG. 2. The Li^6 elastic peak observed at 426 Mev and 45°.

of the entrance slit of the spectrometer ($\sim \pm 1.0^\circ$). When comparing areas of the peaks, suitable correction was made for the narrowness of the Li^6 peaks. This correction corresponds to a calculation of the fraction of the total cross section which was missed because of

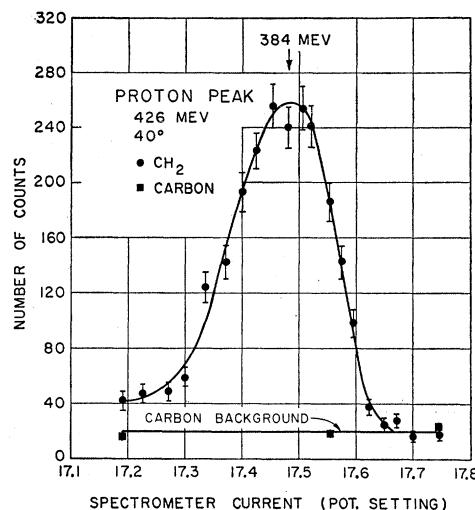


FIG. 3. The elastic "proton" peak observed at 426 Mev and 40°. The target used was polyethylene (CH_2) 237 mils thick. The carbon background points were taken with an equivalent carbon target.

radiation. In other words, both the Li^6 peaks and the proton peak were extended to lower energies by employing the Schwinger and straggling corrections.³ For the Li^6 peak, ΔE was taken to be the energy difference between the center of the peak and the point on the lower energy side of the peak where the counting rate fell to $\frac{1}{3}$ the peak value. Thus $\Delta E/E$ was generally found to be of the order of 0.2%. For the proton ΔE was taken to be the energy difference between the center of the peak and the lowest energy experimental point taken, which was at a potentiometer setting of 17.19, as indicated in Fig. 3. Thus for the proton peak $\Delta E/E$ was 1.23%. These corrections amounted to about 34% for the Li^6 peaks and to 22.7% for the proton peak. Other determinations of the absolute cross sections were made on two separate occasions. The results were consistent, within experimental error, with the results given here.

Table I presents the differential cross section data

TABLE I. Theoretical and experimental cross sections, with radiative corrections, for Li^6 at 426 Mev. Also shown are q values and the experimental values of $F^2(q)$.

I	II	III	IV	V	VI	VII	VIII
θ	$(d\sigma/d\Omega)_{\text{exp}}$ (in units of $10^{-32} \text{ cm}^2/\text{sterad}$)	Schwinger correction (percent)	Bremsstrahlung correction (percent)	Statistical error (percent)	$(d\sigma/d\Omega)_{\text{point}}$ (in units of $10^{-30} \text{ cm}^2/\text{sterad}$)	q (in units of 10^{19} cm^{-1})	$F^2(q)$
33°	149	31.4	3.0	10	34.9	1.22	0.0427
35°	91.4	31.5	3.0	10	28.2	1.30	0.0324
37.5°	43.1	31.8	3.1	10	21.1	1.39	0.0204
40°	24.1	35.4	3.3	10	16.3	1.47	0.0148
41.25°	17.7	31.9	3.0	10	14.4	1.51	0.0123
42.5°	11.4	34.9	3.3	11	12.5	1.56	0.00912
45°	6.45	33.9	3.2	10	10.0	1.65	0.00645
47.5°	2.89	34.7	3.3	11	8.00	1.74	0.00361
50°	1.49	34.6	3.3	12.5	6.45	1.80	0.00231
52.5°	0.776	33.9	3.1	10	5.25	1.88	0.00148
55°	0.330	36.2	3.2	15	4.31	1.97	0.000766
57.7°	0.211	33.7	3.1	13	3.57	2.05	0.000591

TABLE II. Charge distributions and form factors for models which were tried. Parameters which gave the best fit for the three successful models are also shown.

Name of model	$\rho(r)$; a = rms radius	$F(q)$
(1) Gaussian	$\frac{3}{4\pi a^3} \left(\frac{6}{\pi}\right)^{\frac{1}{2}} \exp\left(-\frac{3r^2}{2a^2}\right)$	$\exp\left(-\frac{q^2 a^2}{6}\right)$
(2) Harmonic-well shell model	$\frac{1}{2\pi^{\frac{1}{2}} a^3} \frac{k^3}{(2+3\alpha)} \left(1 + \frac{\alpha k^2 r^2}{a^2}\right) \exp\left(-\frac{k^2 r^2}{a^2}\right)$ where $\alpha = \frac{Z-2}{3} = \frac{1}{3}$, $k^2 = \frac{3(2+5\alpha)}{2(2+3\alpha)} = \frac{11}{6}$	$\left(1 - \frac{\alpha q^2 a^2}{2k^2(2+3\alpha)}\right) \exp\left(-\frac{q^2 a^2}{4k^2}\right)$
(3) Modified harmonic-well shell model	$\frac{2}{9\pi^{\frac{1}{2}} a^3} \left[\frac{3}{a_1^3} \exp\left(-\frac{r^2}{a_1^2}\right) + \frac{r^2}{a_2^5} \exp\left(-\frac{r^2}{a_2^2}\right) \right]$ where $a = (a_1^2 + \frac{5}{6} a_2^2)^{\frac{1}{2}}$	$\frac{2}{3} \exp\left(-\frac{q^2 a_1^2}{4}\right) + \frac{1}{3} \exp\left(-\frac{q^2 a_2^2}{4}\right) \left(1 - \frac{1}{6} q^2 a_2^2\right)$
(4) Hollow exponential	$\frac{50}{3\pi a^4} r \exp\left(-\frac{(20)^{\frac{1}{2}} r}{a}\right)$	$\left(1 + \frac{q^2 a^2}{60}\right) \left(1 + \frac{q^2 a^2}{20}\right)^{-2}$
(5) Modified exponential	$\frac{27}{8\sqrt{2}\pi a^3} \left(1 + \frac{(18)^{\frac{1}{2}} r}{a}\right) \exp\left(-\frac{(18)^{\frac{1}{2}} r}{a}\right)$	$\left(1 + \frac{q^2 a^2}{18}\right)^{-2}$
(6) Fermi 2-parameter	$\frac{\rho_1}{\exp[4.40(r-c')/t'] + 1}$	

	Parameters for best fit (in units of 10^{-13} cm)	Rms radius (in units of 10^{-13} cm)	c (in units of 10^{-13} cm)	t' (in units of 10^{-13} cm)
(1)	No fit
(2)	No fit
(3)	$a_1 = 2.65, a_2 = 1.07$	2.82	1.99	1.75
(4)	$a = 2.80$	2.80	1.92	1.97
(5)	No fit
(6)	$c' = 1.20, t' = 3.10$	2.86	1.43	2.50

already corrected for the radiative and straggling losses (bremsstrahlung). The following quantities are given in this table:

- (1) Column I: The laboratory angle.
- (2) Column II: The experimental cross section, including corrections.
- (3) Column III: The Schwinger correction which was applied to the experimental cross section.
- (4) Column IV: The bremsstrahlung correction which was applied to the experimental cross section.
- (5) Column V: The statistical error of the experimental cross section, which was based on the number of counts observed at the peak of the curve.
- (6) Column VI: The scattering cross section for a point Li^6 nucleus, given by the Mott formula:

$$\left(\frac{d\sigma}{d\Omega}\right)_{\text{point}} = \left(\frac{Ze^2}{2E_0}\right)^2 \frac{\cos^2(\theta/2)}{\sin^4(\theta/2)} \left(1 + \frac{2E_0}{Mc^2} \sin^2(\theta/2)\right)^{-1},$$

when E_0 is the energy of the incident electrons and M is the mass of the Li^6 nucleus.

- (7) Column VII: The momentum transferred by the

electron to the recoil nucleus, which is given by

$$q = \frac{2}{\lambda} \sin(\theta/2) \left(1 + \frac{2E_0}{Mc^2} \sin^2(\theta/2)\right)^{-\frac{1}{2}},$$

where λ is the (reduced) de Broglie wavelength of the incident electrons.

(8) Column VIII: The experimental (form factor)², which is a function of q and is given by the ratio of the experimental cross section (Col. II) to the point cross section (Col. VI). The form factor is the Fourier transform of the charge distribution and is a function of q . It is given by

$$F(q) = \int \rho(r) e^{iq \cdot r} d^3r.$$

A discussion of these formulas is given in references 3 and 4.

III. INTERPRETATION OF THE DATA

Because the Li^6 nucleus has an atomic number of $Z=3$, the Born approximation may be used with considerable confidence in interpreting the angular dis-

tribution in terms of a phenomenological charge distribution. The Born approximation is particularly appropriate in the angular region preceding the first diffraction minimum. (See Fig. 4 of reference 4.) The error anticipated in the use of the Born approximation is less than 1%.

Several phenomenological models have been tried in attempting to fit the data. They are listed in Table II. The gU model of Helm⁶ was also tried without success. Other unsuccessful attempts involved the following models: uniform, exponential, Model VII (Table I of reference 3), and the hollow Gaussian, Model XI (Table I of reference 3).

The form factor for the modified harmonic-well shell model was taken from Tassie.⁷ The calculations for the Fermi 2-parameter model were kindly carried out for us by Meyer-Berkhout using the code and methods of Yennie, Ravenhall, and Wilson.⁸ Thus the Fermi-model calculations are exact.

Charge distribution curves for the three best-fitting models, namely (3), (4), and (6), are shown in Fig. 4.

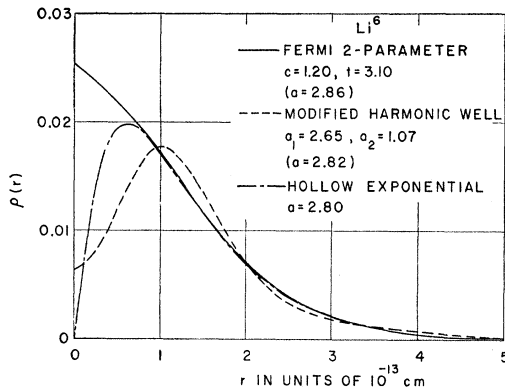


FIG. 4. Charge distribution curves for the three best-fitting models.

In Table II we also show values of c and t for these models. c is the distance to the half-density radius and t is the 10–90% skin thickness.⁹ For models without a flat region at the origin or with structure at the origin the previous definitions of c and t are ambiguous. For cases of monotonically decreasing charge densities as a function of radius we have chosen c to be the abscissa for which the density has fallen to 50% of its value at the origin and t is taken to be the distance between 90% and 10% of the values of the charge density at the origin. For other models we have taken a mean of the charge density over the first 10^{-13} cm from the origin. We have then defined c and t in terms of 50%, 90%, and 10% of this mean value. It should be pointed out that the c and t values which are found for the Fermi 2-parameter

⁶ R. H. Helm, Phys. Rev. **104**, 1466 (1956).

⁷ L. J. Tassie, Proc. Phys. Soc. (London) **A69**, 205 (1956).

⁸ Yennie, Ravenhall, and Wilson, Phys. Rev. **95**, 500 (1954).

⁹ Hahn, Hofstadter, and Ravenhall, Phys. Rev. **105**, 1353 (1957).

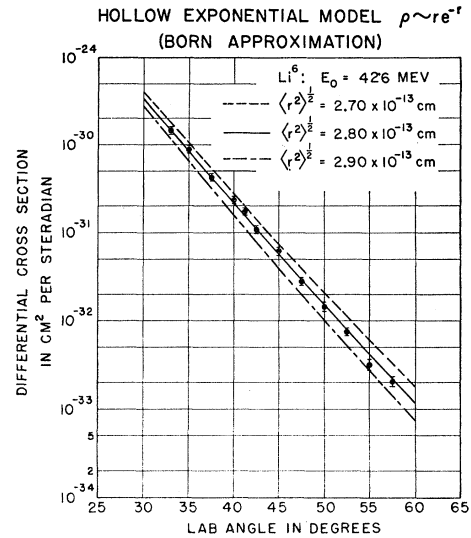


FIG. 5. The experimental cross sections are shown together with theoretical curves for a hollow exponential charge distribution. The solid curve is the best fit, and the dashed curves show the tolerances allowed.

distribution are not the same as the “ c ” and “ t ” (called c' and t' in Table II) which are used as parameters in the functional form of the charge distribution given in Table II.

Figures 5 and 6 show two of the models which fit both the absolute value and the “slope” of the experimental angular distribution, together with the tolerances allowed for these models.

However, it proves to be difficult to find a unique charge distribution fitting the angular distribution of Figs. 5 and 6. One of the reasons is that the energy and

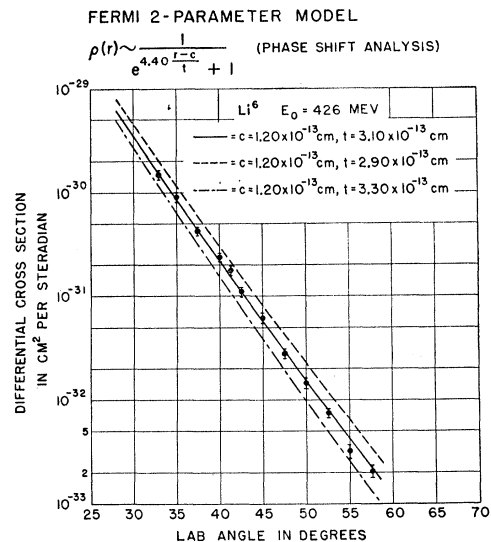


FIG. 6. The experimental cross sections are shown together with theoretical curves for a Fermi 2-parameter charge distribution. The solid curve is the best fit, and the dashed curves show the tolerances allowed.

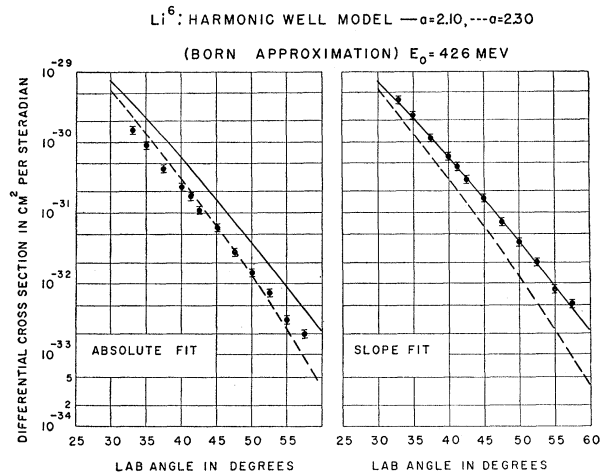


FIG. 7. The experimental cross sections are shown together with theoretical curves for a harmonic-well model charge distribution. The points in the figure on the left are plotted at the *absolute* values experimentally observed; they do not fit the slope of the $a=2.30$ curve. The points in the figure on the right are plotted so as to fit the *slope* of the $a=2.10$ curve; they do not fit the absolute value at 40° .

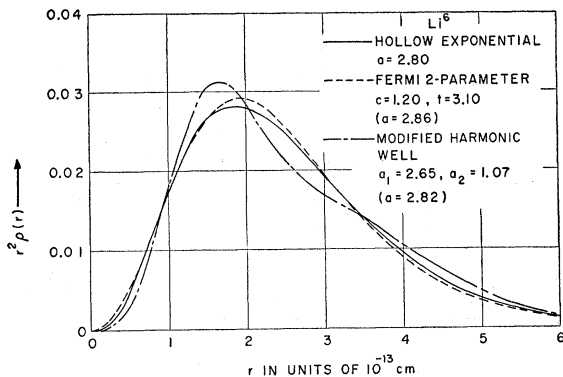


FIG. 8. $r^2\rho(r)$ curves for the three best-fitting models.

angles used in these experiments are not large enough to reach the diffraction minimum. When the latter is reached, e.g., as in the case¹⁰ of C^{12} and O^{16} , the position of this minimum immediately determines a radial parameter, such as an rms radius of the charge distribution. In the case of Li^6 the cross section at this minimum is presently too small to be seen. Hence the fitting procedure must depend on the shape of the angular distribution curve and the absolute value at some fixed position.

Figure 7 shows the harmonic-well model when the parameter $a = \text{rms radius} = 2.30 \times 10^{-13}$ cm is chosen to

¹⁰ Ehrenberg, Hofstadter, Meyer-Berkhout, and Sobottka (to be published).

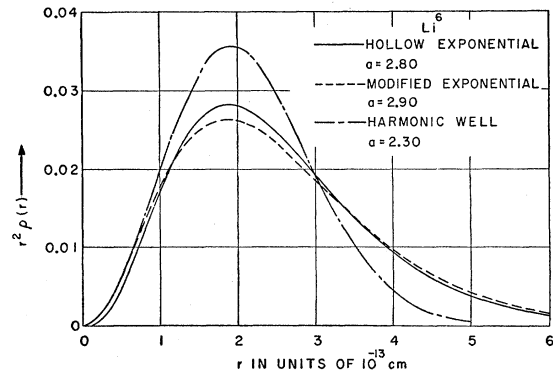


FIG. 9. $r^2\rho(r)$ curves for two unsuccessful models and one successful model (the hollow exponential). The hollow exponential curve is very similar to the modified exponential curve, which, however, does not fit the data.

fit the absolute cross section at 40° . It may be seen, however, that the slope of the curve fits the value $a = 2.10 \times 10^{-13}$ cm although the absolute value does not. It has not been possible to find parameters for a harmonic-well model that fit *both* slope and absolute value within our experimental error. Our first determinations² were based almost entirely on the slope fit, which are now seen to be inconsistent with a fitting of the absolute cross section. Using both slope and absolute value we have been able to eliminate many models such as (1), (2), (5), and others. We have tried to determine properties common to the successful models and also those properties which eliminate unsuccessful models. To make the comparison easier we have plotted in Fig. 8 the $r^2\rho(r)$ curves for the successful models and in Fig. 9 $r^2\rho(r)$ for unsuccessful models along with one successful model (4). These curves are all normalized so that $4\pi \int_0^\infty \rho(r)r^2 dr = 1$.

It may be seen that the successful models all have similar shapes but some unsuccessful models, in particular the modified exponential model, give charge distributions unexpectedly similar to the successful models. Apparently there are delicate differences which distinguish between successful and unsuccessful models.

We have not been able to find a single and unique charge distribution for Li^6 at this time. However, model (4) certainly represents a close approximation. Since we have given the experimental form factors in Table II, these form factors may often be used in lieu of a charge density model. The theoretical problem of determining a unique (within experimental error) charge distribution from experimental data is one that we have not yet solved. This problem may not be resolved without the addition of further experimental data.